Title
Accelerated whole-heart coronary MRA using motion-corrected sensitivity encoding with three-dimensional projection reconstruction

Journal
Magnetic Resonance in Medicine, 73(1)

ISSN
0740-3194

Authors
Pang, Jianing
Sharif, Behzad
Arsanjani, Reza
et al.

Publication Date
2015

DOI
10.1002/mrm.25097

Peer reviewed

Accelerated Whole-Heart Coronary MRA Using Motion-Corrected Sensitivity Encoding with Three-Dimensional Projection Reconstruction

Jianing Pang[1,2], **Behzad Sharif**[2], **Reza Arsanjani**[2], **Xiaoming Bi**[3], **Zhaoyang Fan**[2], **Qi Yang**[4], **Kuncheng Li**[4], **Daniel S. Berman**[2], and **Debiao Li**[2,5,*]

[1]Department of Radiology and Biomedical Engineering, Northwestern University, Chicago, Illinois, USA

[2]Biomedical Imaging Research Institute, Cedars-Sinai Medical Center, Los Angeles, California, USA

[3]MR R&D, Siemens Healthcare, Los Angeles, California, USA

[4]Xuanwu Hospital, Capital Medical University, Beijing, China

[5]University of California, Los Angeles, California, USA

Abstract

Purpose—To achieve whole-heart coronary magnetic resonance angiography (MRA) with (1.0 mm)^3 spatial resolution and 5 min of free-breathing scan time.

Methods—We used an electrocardiograph-gated, T2-prepared and fat-saturated balanced steady state free precession sequence with 3DPR trajectory for free-breathing data acquisition with 100% gating efficiency. For image reconstruction, we used a self-calibrating iterative SENSE scheme with integrated retrospective motion correction. We performed healthy volunteer study to compare the proposed method with motion-corrected gridding at different retrospective undersampling levels on apparent signal-to-noise ratio (aSNR) and subjective coronary artery (CA) visualization scores.

Results—Compared with gridding, the proposed method significantly improved both image quality metrics for undersampled datasets with 6000, 8000, and 10,000 projections. With as few as 10,000 projections, the proposed method yielded good CA visualization scores (3.02 of 4) and aSNR values comparable to those with 20,000 projections.

Conclusion—Using the proposed method, good image quality was observed for free breathing whole-heart coronary MRA at (1.0 mm)^3 resolution with an achievable scan time of 5 min.

Keywords

coronary MRA; sensitivity encoding; motion correction; 3D radial acquisition

[*]Correspondence to: Debiao Li, Ph.D., Biomedical Imaging Research Institute, Cedars-Sinai Medical Center, 8700 Beverly Blvd, PACT Suite 800, Los Angeles, CA, USA 90048. debiao.li@cshs.org.

Additional Supporting Information may be found in the online version of this article.

INTRODUCTION

Current coronary magnetic resonance angiography (MRA) techniques are limited by several factors that impede their routine application in clinical practice, among which are spatial resolution, scan time and robustness to respiratory motion. Three-dimensional projection reconstruction (3DPR) offers multiple advantages for coronary MRA such as high isotropic resolution, wide spatial coverage, mild undersampling artifacts, reduced sensitivity to motion and self-navigation properties (1-4). The shorter achievable repetition time (TR) also helps reduce off-resonance banding artifacts in balanced steady state free precession (bSSFP) imaging, especially at 3 Tesla (T) (5). It has also been shown recently that 3DPR can be combined with retrospective image-based motion correction to achieve 100% acquisition efficiency, enabling whole-heart coronary MRA with high isotropic resolution and significantly shorter scan time (6,7). The current method for reconstructing 3DPR data is the so-called gridding method, which involves convolving the non-Cartesian k-space data with a kernel, resampling the convolved k-space onto a Cartesian grid, transforming the resulting Cartesian k-space into image space by means of Fast Fourier Transform, and finally deapodizing in image space to cancel the effect of the convolution. Taking advantage of the relatively mild undersampling artifacts, previous works have used between 12,000 and 26,000 projections to achieve spatial resolutions of around $(1.15\ \mathrm{mm})^3$ (1-4). However, with more aggressive angular undersampling, gridding results in significant aliasing artifacts that appear as noise-like streaking and reduce the apparent signal-to-noise ratio (aSNR) of the reconstructed image. These artifacts deteriorate the image quality and therefore limit the utility of undersampling as a means of further scan time reduction.

Sensitivity encoding (SENSE) (8) uses the receiver coil sensitivity information that complements Fourier encoding to suppress aliasing artifacts at a cost of amplified reconstruction noise. For Cartesian acquisitions, it has been successfully implemented and is in routine use to significantly reduce scan time (8-10). For non-Cartesian trajectories, SENSE has also been proven effective and is usually accomplished by inverting the encoding matrix using iterative methods such as conjugate-gradient (CG) (11). A key requirement for any SENSE-type methods is accurate coil sensitivity information. This is conventionally obtained from a separate low-resolution calibration scan, which consumes extra time and can be susceptible to misregistration between the sensitivity maps and the actual image. For Cartesian acquisitions, self-calibration can be achieved by estimating the sensitivity maps from a fully sampled central k-space, albeit at a cost of reducing the effective acceleration (12). For most non-Cartesian trajectories, including 3DPR, the k-space central region is oversampled and hence can be used to reconstruct alias- free low-resolution images for sensitivity map estimation without INCURRING EXTRA SCAN TIME. THIS HAS BEEN DEMON-strated for 2D radial and spiral trajectories (13).

In this work, we propose to combine our previously developed 3DPR-based respiratory motion correction framework (7) with self-calibrating CG-SENSE reconstruction. Our retrospective motion correction framework enables 100% respiratory gating efficiency, thereby achieving a fixed scan time regardless of the subject’s breathing pattern. The employed CG-SENSE reconstruction scheme suppresses the streaking artifacts due to

NIH-PA Author Manuscript

NIH-PA Author Manuscript

undersampling effects by exploiting the redundancies in the multichannel dataset. We conduct in vivo studies on healthy volun-teers (N ^{1}/4 9) using a free-breathing bSSFP whole-heart coronary MRA protocol. The image quality is measured for multiple retrospective undersampling levels in terms of the aSNR and the subjective coronary artery (CA) visualization score. We compare the performance of the proposed method with conventional reconstruction (motion-corrected gridding, square root of sum of squares channel combination). Finally, we explore the achievable scan time reduction by determining the appropriate undersampling level that maintains good image quality.

METHODS

Motion-Corrected 3DPR Sensitivity Encoding

Several works have combined retrospective motion correction with sensitivity encoding in cardiac imaging applications (14-18). In this work, we use a two-step procedure for the proposed motion-corrected CG-SENSE reconstruction.

The first step follows our previous respiratory motion-correction work (7). With the cardiac motion suppressed by electrocardiograph (ECG) gating, the free-breathing dataset is segmented into different respiratory bins using self-navigation. With one bin being the reference, the respiratory motion of all other bins is estimated using image-based 3D affine registration, which has been shown to be a good approximation of the respiratory motion (19). Finally, the motion correction is accomplished by using the estimated translation vectors and affine transform matrices to modify the k-space data and trajectory.

In the second step, the motion-corrected k-space data and trajectory is incorporated into the CG-SENSE reconstruction framework as described in (11). For sensitivity self-calibration, we first reconstruct the motion-corrected individual coil images by gridding. We then calculate the coil sensitivity maps using Walsh's method (20,21), which uses the eigenvector of the local signal covariance matrices as the estimate of the respective sensitivity values at the specific spatial location. We average the local image covariance matrices over 20 × 20 × 20 mm^3 blocks to suppress the streaking artifacts. The averaging operation is implemented in MATLAB (The MathWorks, Natick, MA) using the graphical processing unit (GPU), which provided more than 50-fold acceleration compared with regular central processing unit (CPU) implementations. The noise covariance matrix in the SENSE framework is assumed to be an identity matrix. The sensitivity encoding operation is carried out using the gridding/regridding approach with a density compensation function (DCF) iteratively calculated from the k-space trajectory to compensate for sampling nonuniformity (22). Preconditioning by density compensation (11) is used to significantly accelerate convergence of the CG iterations.

Stopping Criterion of the CG Iterations

The SENSE encoding matrix is generally ill-conditioned. However, the CG method is intrinsically regularized with the iteration number effectively acting as a regularization parameter. As a result, the CG-SENSE reconstruction demonstrates a weak convergence behavior: the iterations initially converge toward a solution with a certain image quality, but with subsequent iterations the aSNR deteriorates due to noise amplification (23). In our experiments, we empirically found that a normalized residual of $\delta = 0.01$ yields the overall best trade-off between regularization and noise amplification. In the reconstructed datasets, this residual level corresponded to 20–25 CG iterations, depending on the degree of k-space undersampling. Figure 1 shows the effect of iteration number on image sharpness and aSNR.

Retrospective Undersampling

In this work, we perform retrospective undersampling to avoid the potential inter-scan variability associated with prospectively acquiring multiple undersampled datasets. The k-space trajectory is a slightly modified version of the "spiral on the sphere" (24) trajectory used in several previous works (1,2,6,7). Specifically, the k-space is divided into M interleaves, each one acquired over a certain number of heartbeats and containing N projections, whose origins form a spiral path on a sphere from one pole to the equator. The respective gradients are given by:

$$\begin{aligned} Gz(n) &= \tfrac{(N-n)+0.5}{N} \\ Gx(n) &= cos\left(\tfrac{\sqrt{2N\pi}}{M} sin^{-1}(Gz(n)) + m\theta_{GA}\right)\sqrt{1-Gz(n)^2} \\ Gy(n) &= sin\left(\tfrac{\sqrt{2N\pi}}{M} sin^{-1}(Gz(n)) + m\theta_{GA}\right)\sqrt{1-Gz(n)^2} \end{aligned} \quad [1]$$

where m = 1, 2, 3 … M, n = 1, 2, 3 … N, and θ_{GA} is the 111.25° golden-angle, by which each of the M interleaves is rotated azimuthally with respect to the preceding one. We additionally set the azimuthal coverage of each interleaf to be 180° to traverse k-space frequently, therefore ensuring each respiratory bin to have uniform k-space coverage (6), at the same time minimizing the gradient jump to reduce eddy-current artifacts. With the golden-angle azimuthal increments between interleaves, the retrospective under-sampling is achieved by simply throwing away all heartbeats after the first N_i projections. As shown in the 10,000 projection example in Figure 2, prospective and retrospective undesampling display slightly different sampling patterns. To measure the sampling uniformity, we calculate the relative standard deviation (RSD) of the distances between the projections' origins and their four nearest neighbors (3). As shown in Figure 2c, depending on the number of projections, retrospective undersampling can have either higher or lower RSD than their prospective counterparts. Based on our experience, the resulting changes in the respective point-spread-functions (PSF) and hence aliasing patterns have minimal effect on the final image quality, as shown by the example in Figure 2d.

Undersampling Factor Considerations

The 3DPR trajectory typically contains significantly fewer projections than what is required for alias-free imaging set by the Nyquist criterion (25). Effectively, a uniform angular undersampling reduces the size of the alias-free field of view (FOV) in the image domain according to the following square-root relationship with respect to the number of acquired projections:

$$FOV_{\text{alias-free}} \propto \sqrt{N_{proj}} \quad [2]$$

NIH-PA Author Manuscript

NIH-PA Author Manuscript

To accommodate the wide spatial coverage from the nonselective excitation, we used a matrix size of 384^3 and an isotropic FOV of 400 mm to minimize aliasing along the readout direction from peripheral signal sources such as the arms, the neck and the abdomen. Based on this matrix size, the number of projections to fulfill the Nyquist criterion is approximately 232,000, which is far from achievable in practice. However, assuming adequate magnetization-preparation across the excitation volume, the fat and muscle tissue will appear much darker than the brightest pixels from the ventricular blood pool. Therefore, streaks originating from the peripheral signal sources have lower intensity and consequently have minimal impact on the image quality within the central region-of interest (ROI). Because the heart spans less than one-third of the full FOV in all three dimensions, a relatively alias-free ROI can still be obtained if the alias-free FOV (Eq. [2]) is larger than the size of the heart. Based on this observation, we use 20,000 projections in the in vivo experiments as the maximally sampled reference, corresponding to an alias-free FOV size of 120 mm and approximately 10 min of scan time. As an initial test, retrospective undersampling was performed on one maximally sampled dataset in 2000 projection decrements. Each dataset were then reconstructed using the proposed CG-SENSE method, which were visually evaluated by an experienced reader to determine the required number of projections to achieve various image qualities relative to the reference (N_0): comparable to reference (N_1), lower but acceptable (N_2), and nondiagnostic (N_3). Gridding reconstruction was also performed for comparison.

Another potential source of image quality degradation is the accuracy of respiratory motion estimation. As suggested by previous works (6,7), around 40 heartbeats or 1000 projections are required in each respiratory bin for accurate image based motion estimation. Considering the distribution of data among the current six-bin setup is usually nonuniform, going below 10,000 projections will potentially lead to residual motion blurring due to inadequate motion correction for one or more respiratory bins. Example data distributions for different numbers of projections can be seen in the supplementary material available online.

In Vivo Experiments

Whole-heart coronary MRA data were collected on a clinical 1.5T scanner (MAGNETOM Avanto, Siemens AG Healthcare, Erlangen, Germany) using an ECG gated, T2-prepared and fat-saturated bSSFP pulse sequence with 3DPR trajectory and a 12-channel receiver coil array with the following parameters: TR TE=3.2/1.6 ms, FOV = 400 mm^3, matrix size=384^3, 200 μs =nonselective hard pulse, flip angle=90°, readout bandwidth = 900 Hz/pixel (7). Simple gradient delay correction was performed prospectively (26). A four-chamber CINE image was acquired after the initial localizers to determine the start and duration of the cardiac quiescent period. The cardiac trigger delay and the segment length were adjusted accordingly. No prospective respiratory gating was performed. A total number of 9 healthy volunteers (5 women, average age 29.2 ± 9.1 years) were scanned with IRB approval and written consent. As discussed above, the maximally sampled dataset with N_0 = 20,000 projections was acquired for each subject. Retrospective undersampling was performed resulting in projection numbers N_1, N_2, and N_3. The resultant four datasets were then reconstructed offline using both the proposed method and motion-corrected gridding.

Offline reconstruction was implemented in MATLAB with around eight-fold computational acceleration using parallel computing toolbox on a workstation with a 12-core Intel Xeon CPU, 96 GB of memory, and an Nvidia Tesla C2050 GPU. The coronary images were reformatted using the CoronaViz software (Siemens Corporate Research, Princeton, NJ). Subjective quality scores for all three major coronary artery branches, i.e., left anterior descending (LAD), left circumflex (LCX), and right coronary artery (RCA), were evaluated by two experienced readers blinded to the protocols on a four-point scale: 1: Poor, 2: Fair, 3: Good, 4: Excellent. The scores from the two readers were averaged before statistical analysis. Similar to several previous works on non-Cartesian coronary imaging (1,27,28), we used aSNR as a quantitative measure of the overall image quality. The aSNR is calculated as the ratio between the blood signal intensity, measured within a circular ROI in the aorta at the level of the left coronary ostium, and the apparent noise level which is a blend of "true" noise and noise-like streaking and estimated from the signal standard deviation (SD) in an ROI placed on background air. A nonparametric statistical test (Wilcoxon's signed rank) was used for analyzing the subjective scores, and Student's t-test was used for analyzing aSNR measurements. We used 0.05 as the *P*-value threshold of statistical significance.

RESULTS

As the 3DPR dataset became increasingly undersampled, gridding showed a higher level of streaking artifacts that rapidly deteriorated the aSNR. In contrast, the proposed method largely maintained the image quality down to around 8000 projections, although more aggressive undersampling resulted in noticeable image blurring. With the proposed method, as few as 10,000 projections provided visually identical image quality compared with the reference image with 20,000 projections; with 8000 projections, reduced but still acceptable image quality was observed; yet further undersampling degraded the image quality to nondiagnostic. Therefore we set N_1 to be 10,000 projections, N_2 to be 8,000 projections, and N_3 to be 6000 projections. The example shown in Figure 3 demonstrates these observations in an example dataset.

The imaging time of N_0 and the effective imaging times for N_1 – N_3, defined as the sum of the duration of the heartbeats that would have been required by the shortened acquisition, were as follows: 10.2 ± 1.0 min (N_0), 5.1 ± 0.5 min (N_1), 4.1 ± 0.4 min (N_2), and 3.1 ± 0.3min (N_3). The average aSNR values were 18.7 ± 3.6 (gridding, N_0) and 18.8 ± 4.3 (proposed, N_0), 13.7 ± 2.7 (gridding, N_1) and 17.5 ± 3.5 (proposed, N_1), 12.8 ± 2.8 (gridding, N_2) and 16.6 ± 3.4 (proposed, N_2), and 10.3 ± 1.5 (gridding, N_3) and 15.5 ± 4.4 (proposed, N_3). For each projection number, the images reconstructed by the proposed method showed significantly higher aSNR than those by gridding. Notably, with the proposed reconstruction, the average aSNR of N_1 showed no significant difference compared with N_0, despite the two-fold undersampling. N_2 and N_3, however, showed significantly lower aSNR compared with N_0. The average coronary artery (CA) visualization scores were 3.11 ± 0.39 (gridding, N_0) and 3.26 ± 0.38 (proposed, N_0), 2.50 ± 0.34 (gridding, N_1) and 3.02 ± 0.41 (proposed, N_1), 2.07 ± 0.24 (gridding, N_2) and 2.31 ± 0.39 (proposed, N_2), and 1.80 ± 0.19 (gridding, N_3) and 2.00 ± 0.21 (proposed, N_3). Again for each projection number, the proposed reconstruction yielded significantly higher average CA visualization scores than gridding. When comparing N_1 and N_0 using the proposed method, the maximally sampled N_0 demonstrated a slight albeit significant advantage over N_1. The average score for N_0 and N_1 were 3.26 and 3.02, respectively. With both scores in the "good" category, this result shows that the image quality was maintained undersampling from 20,000 to 10,000 projections, despite the 50% reduction in scan time. The results are summarized in Figure 4.

Figure 5 shows the reformatted images from three example subjects with different reconstruction methods and numbers of projections. The observed image quality confirms the numerical results: The proposed method yielded superior aSNR and CA visualization compared with gridding, and reducing the number of projections from 20,000 to 10,000 only resulted in minimal degradation in image quality.

DISCUSSION

In this work, we developed a high-resolution free-breathing 3DPR scheme that uses self-calibrating CG-SENSE acceleration and retrospective affine motion correction. We then systematically evaluated the performance of the developed method in whole-heart coronary MRA in terms of aSNR and subjective CA visualization scores at $(1.0\ \text{mm})^3$ spatial resolution and different retrospective undersampling levels. Results of the analysis were used to infer the optimal balance between the undersampling level and image quality. We demonstrated that the proposed method significantly improves the aSNR and CA visualization scores compared with gridding. The achievable scan time was as low as 5 min while maintaining good image quality. In principle, a short acquisition time may also improve the robustness of whole-heart coronary MRA by reducing the chance of respiratory pattern drift, heart rate variation, and involuntary subject movement such as coughing and bulk motion during the scan.

Rather than prospectively acquiring the undersampled datasets separately, we performed retrospective undersampling on each 20,000-projection dataset to minimize the potential inter-scan variability that may confound the results. Based on our experience, the sampling uniformity difference of prospective and retrospective undersampling was not critical in the scope of this work. However, in the presence of the often-conflicting requirements on sampling uniformity, eddy-current minimization, and frequent k-space traverse, trajectory optimization remains as an important topic and warrants continuing efforts.

Notably, no significant drop in aSNR was observed at N_1 = 10,000 projections compared with N_0 = 20,000 projections. Qualitatively speaking, this result indicates that at this particular undersampling level, the streaking suppression from the proposed parallel imaging reconstruction makes up for the accompanying noise amplification. However, using aSNR as a surrogate for true SNR has its limitations, the major one being that true noise and the noise-like streaking are not separated. Furthermore, as the noise amplification varies spatially due to parallel imaging (29), the true noise level in the signal ROI may be different than that of the background ROI. To reduce this potential error, we positioned the background ROI as close to the signal ROI as possible, and used identical coil configurations for all subjects. However, different undersampling factors may have different noise amplification pattern, which we did not account for in our analysis. To better illustrate the trade-off between SNR and acceleration, a more rigorous study on the noise performance of the proposed method is desired in the future.

Several previous investigations have used 3DPR for whole-heart coronary MRA with potential advantages of volumetric coverage and isotropic resolution (1,3), respiratory self-navigation (2,4), and retrospective motion correction (6,7). With gridding reconstruction, the streaking artifacts from angular undersampling adversely affect the image quality. To alleviate this problem, advanced reconstruction strategies have been explored previously, including self-calibrated k-space parallel imaging (GRAPPA) (30) and coil-by-coil compressed sensing (CS) reconstruction with GPU implementation (31). The proposed method uses a flexible k-space motion correction scheme that can be integrated into the CG-SENSE framework in a straight-forward manner. However, other advanced reconstruction methods may also apply. For example, the proposed method does not currently impose any explicit L1 regularization, commonly used in CS type reconstructions to exploit image sparsity in certain transform domains. A recent work by Akcakaya et al (32) compared Cartesian CS and parallel imaging, and concluded that the former is more suitable for low SNR applications such as high resolution coronary MRA. Future investigations are warranted to compare the performance of the proposed non-Cartesian parallel imaging method, CS, and potentially a combination of the two. It is also worth exploring the benefit of more sophisticated motion models, such as nonrigid deformation, that may further improve the accuracy of respiratory motion modeling while still can be incorporated into the encoding operations (14).

The proposed method will benefit from coil arrays with more receiver elements, such as a 32-channel coil (33-36), which offer higher baseline SNR and alleviated coil geometry constraints. Additionally, the increased flexibility in selecting different coil elements will help reducing the overall sensitivity to any bright peripheral signal sources, such as insufficiently suppressed fat tissue due to B_0 or B_1 inhomogeneity, and thus lowering the streaking level in the central heart ROI. The major practical issue with using more coil elements is the elevated computational burden. For the 12-channel setup in this work, the complex double coil sensitivity matrix has a size of around 10 GB, and the CG-SENSE reconstruction requires around 80 GB of free memory space. The current reconstruction time is around 1.5–2 h including motion correction, sensitivity map estimation, and the CG-SENSE iterations. To address the memory demand associated with even larger receiver coil arrays, at least two solutions can be explored in the future. First, channel compression can be performed to reduce the computational demand without significant negative effect on image quality (37). Second, by excluding some of the coil elements that are mainly sensitive to peripheral FOV, one can potentially reduce the readout oversampling factor without introducing significant aliasing. Indeed, decreasing the number of readout points from 384 to 256 will shrink the raw image matrix by over 70%, thus greatly alleviating the memory requirement.

Finally, the proposed method offers a flexible frame-work that can be applied to many scenarios that require accelerated acquisition with wide coverage and isotropic resolution. For example, following the successful demonstration in this work on noncontrast coronary MRA, the developed framework can be readily generalized to contrast-enhanced coronary

MRA with inversion-recovery prepared spoiled gradient echo, the current method of choice for 3T (35,38,39). A major challenge with the conventional protocol is that the unpredictable scan time and variable contrast dynamics makes it difficult to synchronize the k-space center acquisition with maximum coronary artery enhancement. With 3DPR, careful prospective timing becomes unnecessary as the contrast dynamics can be retrospectively monitored either from the self-navigation profiles or a series of 3D time-resolved images (40). The data collected during rapid contrast change or the wash out phase can be simply discarded. Meanwhile, effort should be made to optimize the contrast injection strategy to maintain a stable blood pool enhancement during the scan time to minimize significant intensity modulation to the 3DPR k-space or disruption of the self-navigation profiles.

CONCLUSIONS

We have developed a 3DPR based coronary MRA protocol that combines self-calibrating CG-SENSE reconstruction and self-navigated respiratory motion correction with 100% acquisition efficiency. We presented results demonstrating that the proposed method significantly improves the image quality compared with motion-corrected gridding reconstruction. Moreover, the in vivo studies indicate that good image quality can be achieved with 5 min of scan time in healthy volunteers. Future studies are needed to test the clinical utility of the proposed coronary MRA method on a patient population with suspected coronary artery disease, as well as to explore other application areas of the proposed accelerated 3DPR technique.

Acknowledgments

Grant sponsor: NIH; Grant number: HL38698, EB002623; Grant sponsor: National Natural Science Foundation of China; Grant number: 81229001.

REFERENCES

1. Stehning C, Bornert P, Nehrke K, Eggers H, Dossel O. Fast isotropic volumetric coronary MR angiography using free-breathing 3D radial balanced FFE acquisition. Magn Reson Med. 2004; 52:197–203. [PubMed: 15236387]
2. Stehning C, Bornert P, Nehrke K, Eggers H, Stuber M. Free-breathing whole-heart coronary MRA with 3D radial SSFP and self-navigated image reconstruction. Magn Reson Med. 2005; 54:476–480. [PubMed: 16032682]
3. Piccini D, Littmann A, Nielles-Vallespin S, Zenge MO. Spiral phyllotaxis: the natural way to construct a 3D radial trajectory in MRI. Magn Reson Med. 2011; 66:1049–1056. [PubMed: 21469185]
4. Piccini D, Littmann A, Nielles-Vallespin S, Zenge MO. Respiratory self-navigation for whole-heart bright-blood coronary MRI: methods for robust isolation and automatic segmentation of the blood pool. Magn Reson Med. 2012; 68:571–579. [PubMed: 22213169]
5. Xie J, Lai P, Bhat H, Li D. Whole-heart coronary magnetic resonance angiography at 3.0T using short-TR steady-state free precession, vastly undersampled isotropic projection reconstruction. J Magn Reson Imaging. 2010; 31:1230–1235. [PubMed: 20432361]
6. Bhat H, Ge L, Nielles-Vallespin S, Zuehlsdorff S, Li D. 3D radial sampling and 3D affine transform-based respiratory motion correction technique for free-breathing whole-heart coronary MRA with 100% imaging efficiency. Magn Reson Med. 2011; 65:1269–1277. [PubMed: 21500255]
7. Pang J, Bhat H, Sharif B, Fan Z, Thomson LE, Labounty T, Friedman JD, Min J, Berman DS, Li D. Whole-heart coronary MRA with 100% respiratory gating efficiency: self-navigated three-

dimensional retrospective image-based motion correction (TRIM). Magn Reson Med. 2014; 71:67–74. [PubMed: 23401157]

8. Pruessmann KP, Weiger M, Scheidegger MB, Boesiger P. SENSE: sensitivity encoding for fast MRI. Magn Reson Med. 1999; 42:952–962. [PubMed: 10542355]
9. Deshmane A, Gulani V, Griswold MA, Seiberlich N. Parallel MR imaging. J Magn Reson Imaging. 2012; 36:55–72. [PubMed: 22696125]
10. Larkman DJ, Nunes RG. Parallel magnetic resonance imaging. Phys Med Biol. 2007; 52:R15–R55. [PubMed: 17374908]
11. Pruessmann KP, Weiger M, Bornert P, Boesiger P. Advances in sensitivity encoding with arbitrary k-space trajectories. Magn Reson Med. 2001; 46:638–651. [PubMed: 11590639]
12. McKenzie CA, Yeh EN, Ohliger MA, Price MD, Sodickson DK. Self-calibrating parallel imaging with automatic coil sensitivity extraction. Magn Reson Med. 2002; 47:529–538. [PubMed: 11870840]
13. Yeh EN, Stuber M, McKenzie CA, Botnar RM, Leiner T, Ohliger MA, Grant AK, Willig-Onwuachi JD, Sodickson DK. Inherently self-calibrating non-Cartesian parallel imaging. Magn Reson Med. 2005; 54:1–8. [PubMed: 15968671]
14. Batchelor PG, Atkinson D, Irarrazaval P, Hill DL, Hajnal J, Larkman D. Matrix description of general motion correction applied to multishot images. Magn Reson Med. 2005; 54:1273–1280. [PubMed: 16155887]
15. Odille F, Cindea N, Mandry D, Pasquier C, Vuissoz PA, Felblinger J. Generalized MRI reconstruction including elastic physiological motion and coil sensitivity encoding. Magn Reson Med. 2008; 59:1401–1411. [PubMed: 18421689]
16. Odille F, Vuissoz PA, Marie PY, Felblinger J. Generalized reconstruction by inversion of coupled systems (GRICS) applied to free-breathing MRI. Magn Reson Med. 2008; 60:146–157. [PubMed: 18581355]
17. Schmidt JF, Buehrer M, Boesiger P, Kozerke S. Nonrigid retrospective respiratory motion correction in whole-heart coronary MRA. Magn Reson Med. 2011; 66:1541–1549. [PubMed: 21604297]
18. Hansen MS, Sorensen TS, Arai AE, Kellman P. Retrospective reconstruction of high temporal resolution cine images from real-time MRI using iterative motion correction. Magn Reson Med. 2012; 68:741–750. [PubMed: 22190255]
19. Manke D, Nehrke K, Bornert P, Rosch P, Dossel O. Respiratory motion in coronary magnetic resonance angiography: a comparison of different motion models. J Magn Reson Imaging. 2002; 15:661–671. [PubMed: 12112516]
20. Walsh DO, Gmitro AF, Marcellin MW. Adaptive reconstruction of phased array MR imagery. Magn Reson Med. 2000; 43:682–690. [PubMed: 10800033]
21. Griswold, M.; Walsh, D.; Heidemann, R.; Haase, A.; Jakob, P. The use of an adaptive reconstruction for array coil sensitivity mapping and intensity normalization; Proceedings of the 10th Annual Meeting of ISMRM; Honolulu, Hawaii, USA. 2002; Abstract 2410
22. Pipe JG, Menon P. Sampling density compensation in MRI: rationale and an iterative numerical solution. Magn Reson Med. 1999; 41:179–186. [PubMed: 10025627]
23. Qu P, Zhong K, Zhang B, Wang J, Shen GX. Convergence behavior of iterative SENSE reconstruction with non-Cartesian trajectories. Magn Reson Med. 2005; 54:1040–1045. [PubMed: 16149063]
24. Wong ST, Roos MS. A strategy for sampling on a sphere applied to 3D selective RF pulse design. Magn Reson Med. 1994; 32:778–784. [PubMed: 7869901]
25. Barger AV, Block WF, Toropov Y, Grist TM, Mistretta CA. Time-resolved contrast-enhanced imaging with isotropic resolution and broad coverage using an undersampled 3D projection trajectory. Magn Reson Med. 2002; 48:297–305. [PubMed: 12210938]
26. Speier, P.; Trautwein, F. Robust radial imaging with predetermined isotropic gradient delay correction; Proceedings of the 14th Annual Meeting of ISMRM; Seattle, Washington, USA. 2006; Abstract 2379
27. Boubertakh R, Prieto C, Batchelor PG, Uribe S, Atkinson D, Eggers H, Sorensen TS, Hansen MS, Razavi RS, Schaeffter T. Whole-heart imaging using undersampled radial phase encoding (RPE)

and iterative sensitivity encoding (SENSE) reconstruction. Magn Reson Med. 2009; 62:1331–1337. [PubMed: 19780159]

28. Kolbitsch C, Prieto C, Smink J, Schaeffter T. Highly efficient whole-heart imaging using radial phase encoding-phase ordering with automatic window selection. Magn Reson Med. 2011; 66:1008–1018. [PubMed: 21437976]
29. Eggers, H.; Mazurkewitz, P.; Boesiger, P. Noise amplification in non-Cartesian parallel imaging; Proceedings of the 13th Annual Meeting of ISMRM; Miami, Florida, USA. 2005; Abstract 2379
30. Arunachalam A, Samsonov A, Block WF. Self-calibrated GRAPPA method for 2D and 3D radial data. Magn Reson Med. 2007; 57:931–938. [PubMed: 17457884]
31. Nam S, Akcakaya M, Basha T, Stehning C, Manning WJ, Tarokh V, Nezafat R. Compressed sensing reconstruction for whole-heart imaging with 3D radial trajectories: a graphics processing unit implementation. Magn Reson Med. 2013; 69:91–102. [PubMed: 22392604]
32. Akcakaya M, Basha TA, Chan RH, Manning WJ, Nezafat R. Accelerated isotropic sub-millimeter whole-heart coronary MRI: compressed sensing versus parallel imaging. Magn Reson Med. 2013 doi: 10.1002/mrm.24683.
33. Nehrke K, Bornert P, Mazurkewitz P, Winkelmann R, Grasslin I. Free-breathing whole-heart coronary MR angiography on a clinical scanner in four minutes. J Magn Reson Imaging. 2006; 23:752–756. [PubMed: 16557495]
34. Niendorf T, Hardy CJ, Giaquinto RO, et al. Toward single breath-hold whole-heart coverage coronary MRA using highly accelerated parallel imaging with a 32-channel MR system. Magn Reson Med. 2006; 56:167–176. [PubMed: 16755538]
35. Yang Q, Li K, Liu X, Bi X, Liu Z, An J, Zhang A, Jerecic R, Li D. Contrast-enhanced whole-heart coronary magnetic resonance angiography at 3.0-T: a comparative study with X-ray angiography in a single center. J Am Coll Cardiol. 2009; 54:69–76. [PubMed: 19555843]
36. Nagata M, Kato S, Kitagawa K, Ishida N, Nakajima H, Nakamori S, Ishida M, Miyahara M, Ito M, Sakuma H. Diagnostic accuracy of 1.5-T unenhanced whole-heart coronary MR angiography performed with 32-channel cardiac coils: initial single-center experience. Radiology. 2011; 259:384–392. [PubMed: 21406635]
37. Buehrer M, Pruessmann KP, Boesiger P, Kozerke S. Array compression for MRI with large coil arrays. Magn Reson Med. 2007; 57:1131–1139. [PubMed: 17534913]
38. Stuber M, Botnar RM, Danias PG, McConnell MV, Kissinger KV, Yucel EK, Manning WJ. Contrast agent-enhanced, free-breathing, three-dimensional coronary magnetic resonance angiography. J Magn Reson Imaging. 1999; 10:790–799. [PubMed: 10548790]
39. Bi X, Carr JC, Li D. Whole-heart coronary magnetic resonance angiography at 3 Tesla in 5 minutes with slow infusion of Gd-BOPTA, a high-relaxivity clinical contrast agent. Magn Reson Med. 2007; 58:1–7. [PubMed: 17659628]
40. Lai P, Huang F, Li Y, Nielles-Vallespin S, Bi X, Jerecic R, Li D. Contrast-kinetics-resolved whole-heart coronary MRA using 3DPR. Magn Reson Med. 2010; 63:970–978. [PubMed: 20373398]

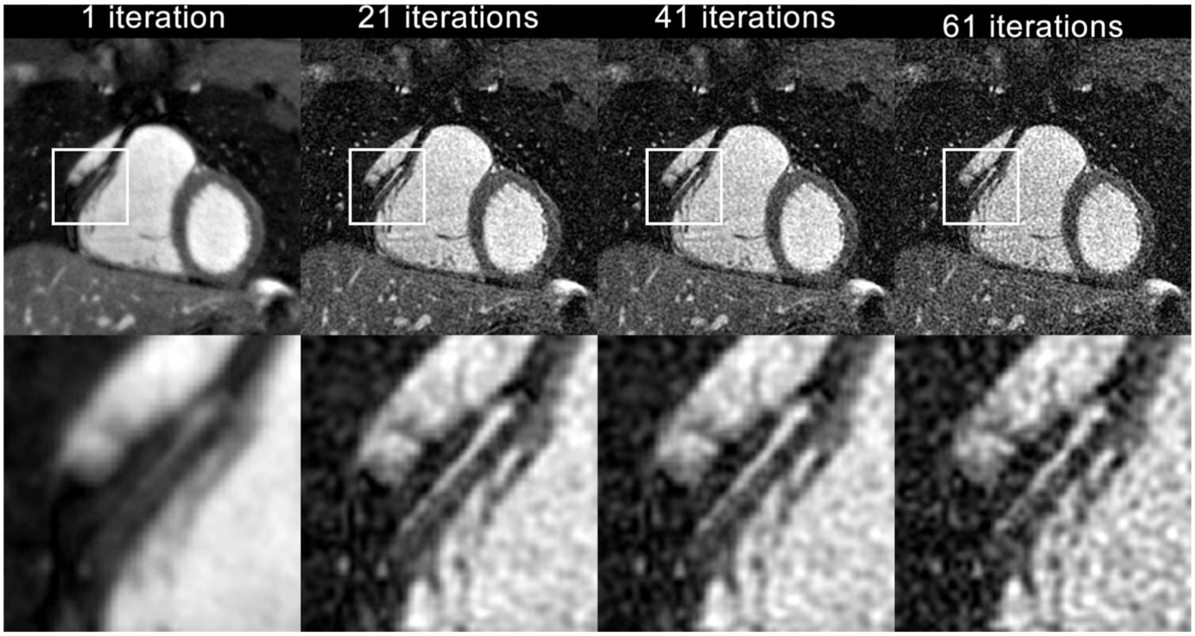

FIG. 1.

An example reconstruction with 10,000 projections showing the effect of iteration number on image sharpness and reconstruction noise. The first several iterations significantly improve the resolution while keeping noise level relatively low. However, after a certain point the additional noise amplification overwhelms any perceptible resolution improvement. For this example, the CG algorithm is stopped at 21 iterations.

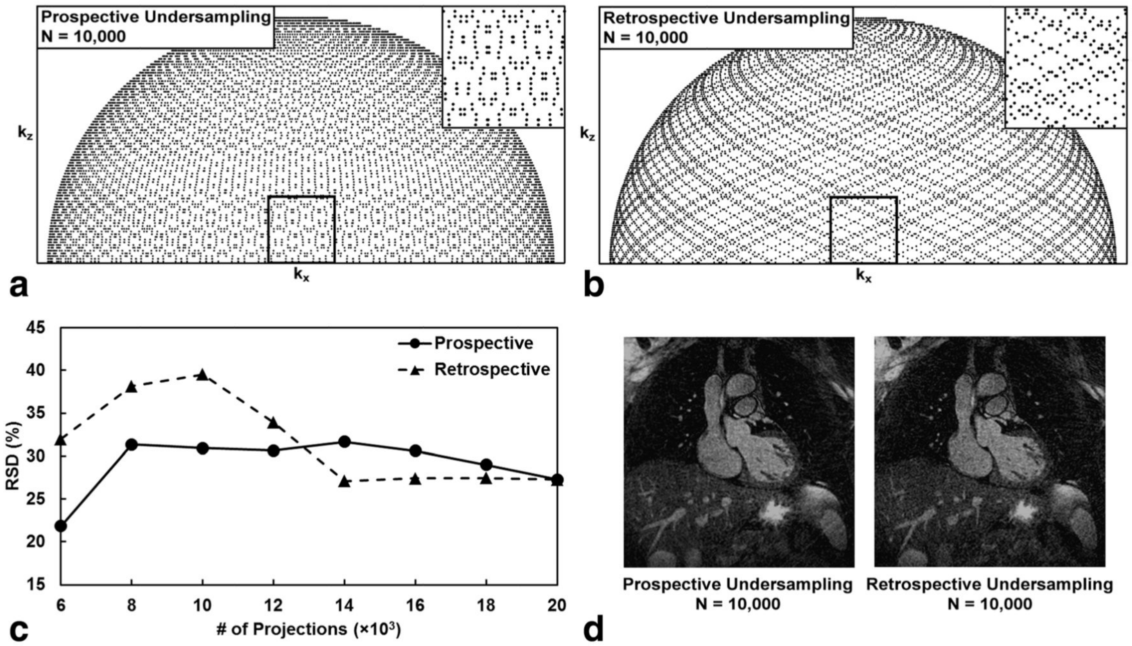

FIG. 2.

Comparing prospective (**a**) and retrospective (**b**) undersampling with N = 10,000 projections. Each dot represents the kx-kz coordinate of the starting point of a projection. The two display slightly different sampling patterns, as can be seen in the zoom-in view. **c**: For different numbers of projections, retrospective (dashed line) and prospective (solid line) undersampling show different RSD values, a measure of sampling uniformity. **d**: Based on our experience, the sampling pattern difference has minimal effect on the final image quality, and should not alter the conclusion of this work.

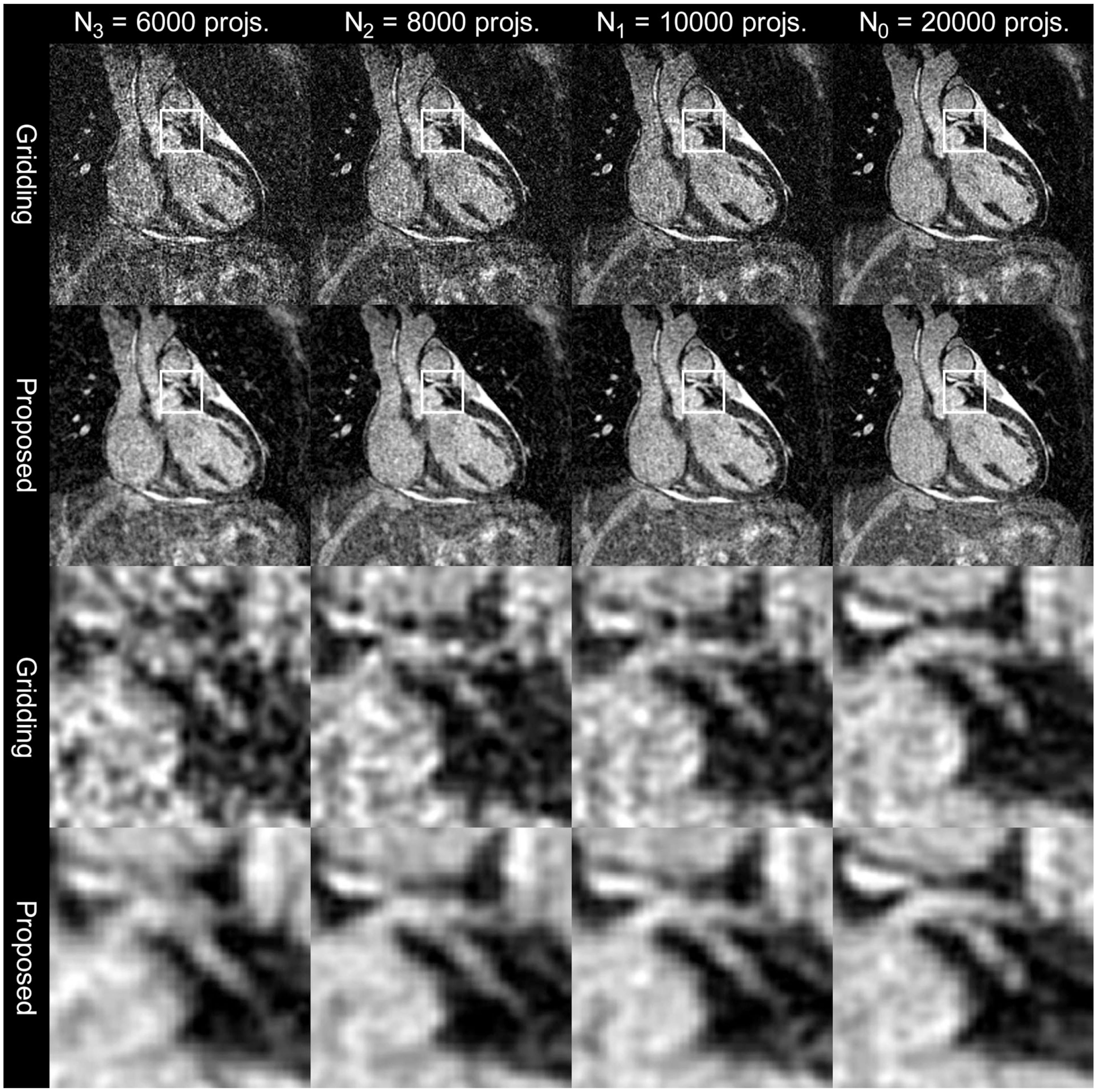

FIG. 3.

Example images reconstructed using gridding (first row) and the proposed method (second row) from 6000, 8000, 10,000 and 20,000 projections, with magnified coronal views of the left main coronary artery. As the projection number reduced, the image quality with gridding quickly degraded, whereas with the proposed method the image quality was largely maintained.

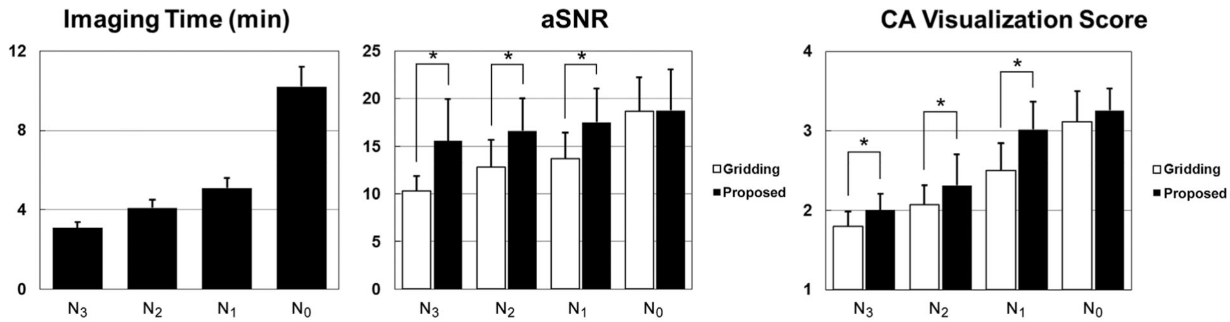

FIG. 4.

Left: Average imaging time for different projection numbers. N_1 (10,000 projections), N_2 (8000 projections), and N_3 (6000 projections) corresponded to scan time reductions by 50%, 61%, and 71% compared with N_0 (20,000 projections), respectively. Middle: Average aSNR values of gridding and the proposed method with different projection numbers. With the exception of N_0, the proposed method significantly improved the aSNR over gridding for a given number of projections. Notably, with the proposed method, there was no significant difference between N_1 and N_0 despite the 50% reduction in scan time. Right: Average CA visualization scores of gridding and the proposed method with different projections numbers. Similarly, the proposed method significantly improved the score compared with gridding with the same number of projections. With the proposed method, N_0 showed a slight albeit significant advantage over N_1 (3.26 versus 3.02, $P = 0.008$). Both scores are considered as good. An asterisk (*) indicates statistical significance ($P < 0.05$).

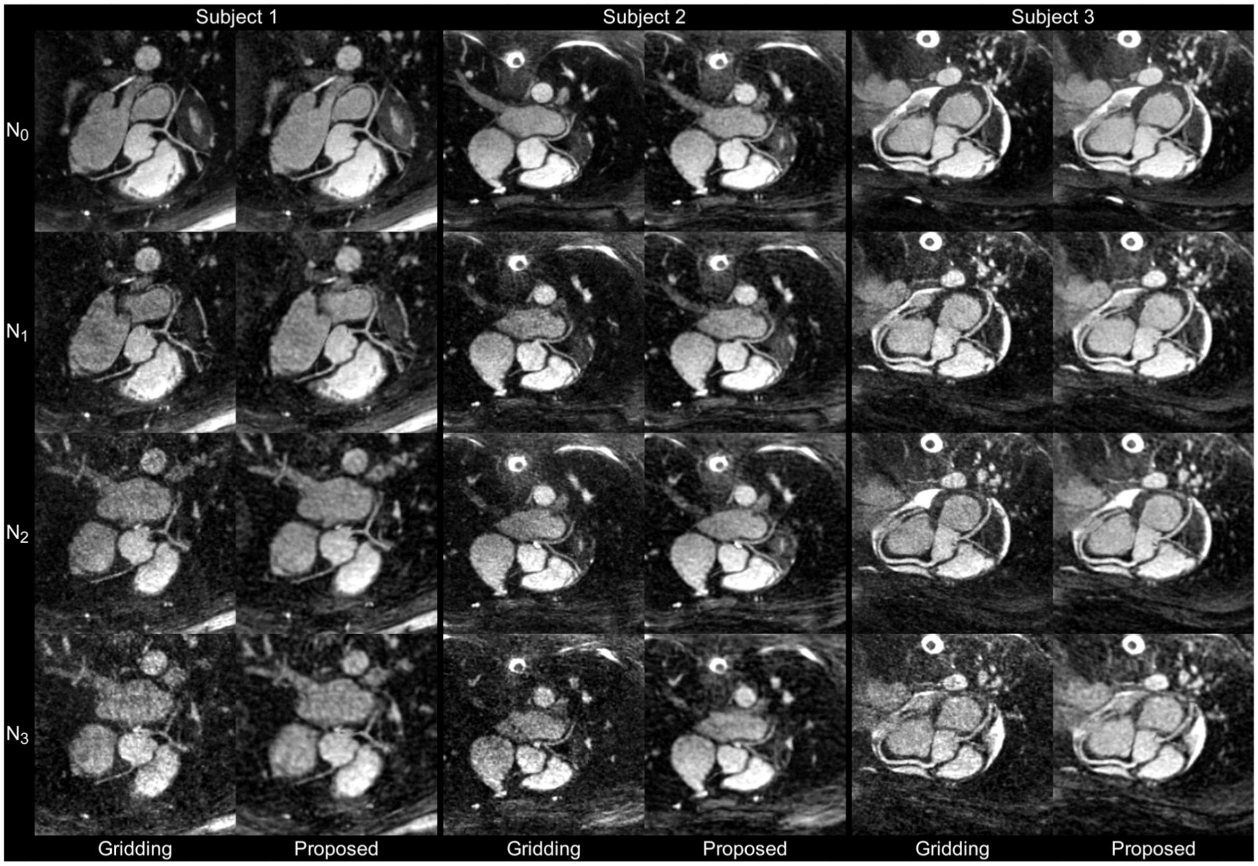

FIG. 5.

Reformatted images of three example subjects reconstructed by gridding and the proposed method with different projection numbers. Visually, the trend in image quality is in accordance with the numerical results. Comparing the two columns of each subject, the proposed method showed superior image quality to gridding. With 10,000 projections, the proposed method offered nearly identical image quality to the maximally sampled image with 20,000 projections.